GeoScienceWorld
Lithosphere
Volume 2022, Article ID 4135908, 17 pages
https://doi.org/10.2113/2022/4135908

Lithosphere

Research Article

Research on the Nucleation Mechanism and Early Warning Method of Strain Rockburst in Deep-Buried Tunnel Based on Microseismic Monitoring

Qun Yu,[1] **Chunyan Bao**,[2] **Shengji Jin**,[1] **and Junxiang Wang**[1]

[1]*School of Architecture and Civil Engineering, Shenyang University of Technology, Shenyang 110870, China*
[2]*School of Civil Engineering, Shaoxing University, Shaoxing 312000, China*

Correspondence should be addressed to Chunyan Bao; fengniaobcy@163.com

Received 15 June 2022; Accepted 30 July 2022; Published 16 August 2022

Academic Editor: Shaofeng Wang

Copyright © 2022 Qun Yu et al. Exclusive Licensee GeoScienceWorld. Distributed under a Creative Commons Attribution License (CC BY 4.0).

In order to discuss the nucleation mechanism of strain rockburst, this paper takes the rockburst section of deep diversion tunnel of Jinping Hydropower Project of Yalong River as the research object. Through the study of microseismic monitoring technology and the regularity of microseismic parameters, as well as combining the qualitative and quantitative analysis, the nucleation process and instability failure mechanism of strain rockburst were revealed, and the internal relationship between microseismic evolution law and rockburst process was explored. The monitoring results and analysis showed that the development process of strain rockburst under engineering disturbance can be divided into three stages: tensile crack initiation and development stage, macroscopic shear crack formation stage, and overall instability stage, respectively. The failure process was mainly that two macroscopic shear cracks caused by tensile failure were connected and developed to the tunnel wall and then formed a closed triangle region. The rock mass in this area appeared plate-like splitting, spalling, and wedge-shaped rock mass ejection at a certain initial velocity, which eventually lead to intense rockburst and overall instability failure. The results also showed that the rockburst failure process under engineering excavation was in good agreement with the traditional syllogism of rockburst. Meanwhile, based on the evolution characteristics of source parameters and statistical parameters, including microseismic energy, moment magnitude, cumulative apparent volume, energy index, and b value, the quantitative interpretation of the source parameter provided significant evidence and insight into characterization of strainbursts. In addition, these parameter fluctuation characteristics can be effectively used as the precursor information and early warning index of strain rockburst failure. The results of this study can provide reference for monitoring and early warning of rockburst in deep tunnel and taking effective prevention and support measures in time.

1. Introduction

In recent years, with the rapid development of water conservancy and hydropower engineering and tunnel engineering in China, the long, large, deep, and group characteristics of underground caverns are becoming more and more obvious, which leads to the increasingly serious engineering geological disasters. Among them, the rockburst problem is the most obvious. During the construction of Qinling tunnel, Sichuan-Tibet highway and Jinping II hydropower station, a large number of rockbursts and economic losses were encountered, which posed a serious threat to the safety of the construction workers. Table 1 lists the basic situation and records of rockburst disasters of key tunnel projects in China and statisticizes the occurrence proportion of rockburst events of different grades and intensities [1]. It can be seen that the rockburst has a high frequency and wide range of influence. Therefore, it has important application value and theoretical significance to carry out the research on strain rockburst nucleation mechanism and warning method of deep-buried tunnel.

The classification and mechanism of rockburst are complicated. It is the basis of effective prediction and early warning of rockburst to correctly identify the types and mechanism of rockburst. According to the origin and mechanism of rockburst, Kaiser and Cai [2] and CRRP [3] divided

Downloaded from http://pubs.geoscienceworld.org/gsa/lithosphere/article-pdf/doi/10.2113/2022/4135908/5676430/4135908.pdf
by guest

Downloaded from http://pubs.geoscienceworld.org/gsa/lithosphere/article-pdf/doi/10.2113/2022/4135908/5676430/4135908.pdf
by guest

Table 1: Incomplete statistical of rockburst record in tunnel engineering in China [1].

Project name	Completion date	Maximum depth/m	Rockburst grades and proportions/%			The frequency of rockburst	Cumulative length of rockburst section/m
			Slight	Medium	Intense~extremely intense		
Diversion tunnel of Tianshengqiao secondary hydropower station	1996	800	70	29.5	0.5	30	—
Qinling railway tunnel	1998	1615	59.3	34.3	6.4	—	1849
Sichuan-Tibet highway Erlang Mountain tunnel	2001	760	Dominant	Slight	None	>200	1252
Lujialing tunnel in Chongqing	2004	600	55.8	39.7	4.5	93	—
Waterfall gully hydropower station into the traffic cave	2005	420	—	—	—	183	—
Qinling Zhongnan Mountain long highway tunnel	2007	1600	61.7	25.6	12.7	—	2664
Jinping-II hydropower station	2011	2525	44.9	46.3	8.8	>750	—
Diversion tunnel of riverside power station	2012	1678	46.4	50.4	3.2	>300	—

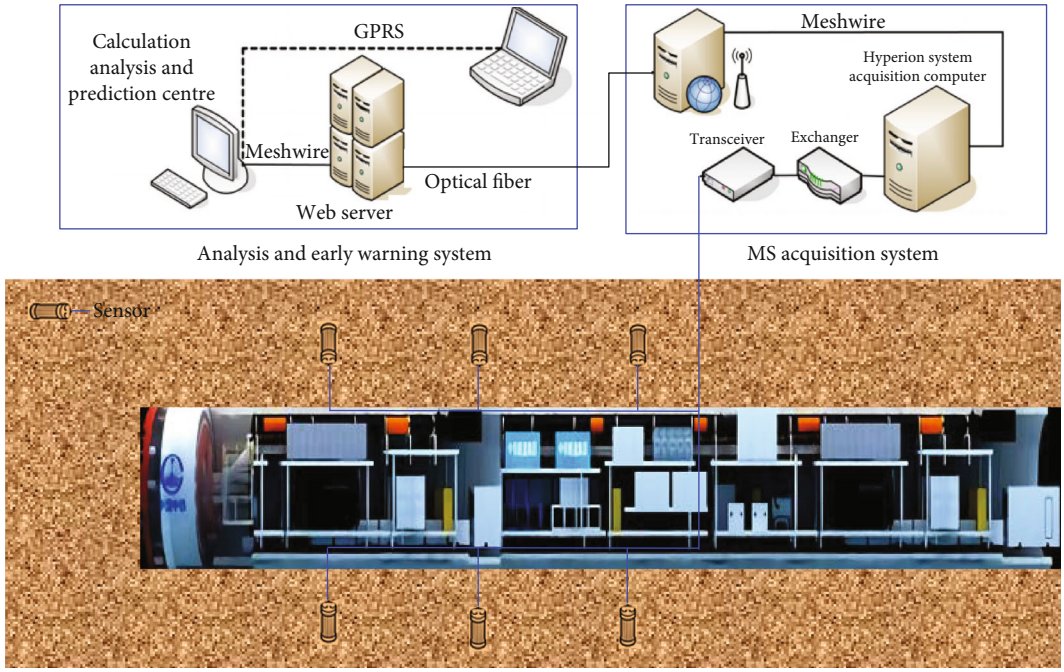

Figure 1: The monitoring and analysis system for rockbursts during TBM tunneling of Jinping II hydropower station.

the rockburst into three types: strain rockburst, tectonic rockburst (or fault-slip rockburst), and pillar rockburst, respectively. The rockburst occurred in Jinping tunnel is mainly strain rockburst [4]. Strain rockburst is caused by local stress concentration and elastic strain energy accumulation and release after excavation disturbance. Stress conditions are critical in deep-buried hard rock tunnels and significantly influence its stability [5]. It often occurs in hard rock tunnels with high stress level and good rock integrity, with high frequency, wide failure range, and failure grades ranging from slight to severe. Therefore, it is of great significance to develop the nucleation mechanism and early warning method of strain rockburst in deep-buried tunnel. At the present stage, in terms of the nucleation and occurrence mechanism of strain rockburst, Tan [6] based on the field investigation believes that the failure surface of strain rockburst is a stepped V-shaped section as a whole, and there are three stages in the failure process of strain rockburst: splitting into plates, shearing into blocks, and block ejection. Gu et al. [7] divided the formation processes of strain rockburst into three stages: tensile splitting, fracture forming, and block ejection through laboratory tests. Through the deep rockburst simulation test system, He et al. [8, 9] believe that the strain rockburst has experienced three processes: vertical plate cracking, vertical plate buckling deformation, and rockburst failure, and they divided the failure process of strain rockburst into four stages: small particle ejection, flaky stripping with mixed particle ejection, massive caving, and overall collapse, respectively. Through the laboratory tests, Chen et al. [10] believed that the occurrence of rockburst was a process of energy accumulation and release. Accordingly, rockburst development processes were divided into three stages: energy accumulation, formation, and propagation of microcracks, crack penetration, and bursting. Xu [11] compared the secondary stress field test of surrounding rock with the whole process of surrounding rock deformation and failure and classified rockburst into compression-induced cracking, compression-induced shear cracking, and bending drum and fold through conventional triaxial unloading test. Wang et al. [12] considered rockburst process consists three progressive steps under the true triaxial test: surface slabbing, rapid ejection and violent burst of chips, and final shear failure. Through the true triaxial rigid testing machine, Su et al. [13] divided the failure process of rockburst ejection into four stages: pellet ejection, splitting into plate, shearing into block, and plate folding ejection. Zhou et al. [14] proposed the mechanism of plate crack buckling of rockburst based on typical rockburst cases of deep-buried tunnels in Jinping Hydropower Project. It is considered that the slab cracking failure occurs in the surrounding rock due to the excavation unloading, and the slab flexures and deforms towards the excavation space and accumulates strain energy. Finally, the sudden instability failure occurs under the action of high stress and disturbance, and the rockburst phenomenon characterized by the slab buckling and rock ejection was formed. Based on laboratory tests, Ma et al. [15] divided the failure process of strain rockburst into three stages: occurrence stage of tensile crack, shear crack, and rockburst caused by cracks connecting with each other, respectively. After that, based on the similar model test, Li et al. [16] concluded that the mechanical mechanism of rockburst process is mainly manifested in three stages: stress concentration stage, energy dissipation stage, transfer and energy storage stage, and instability stage when rock mass releases energy with tensile and shear failure occurs, and finally, rockburst occurs.

Downloaded from http://pubs.geoscienceworld.org/gsa/lithosphere/article-pdf/doi/10.2113/2022/4135908/5676430/4135908.pdf
by guest

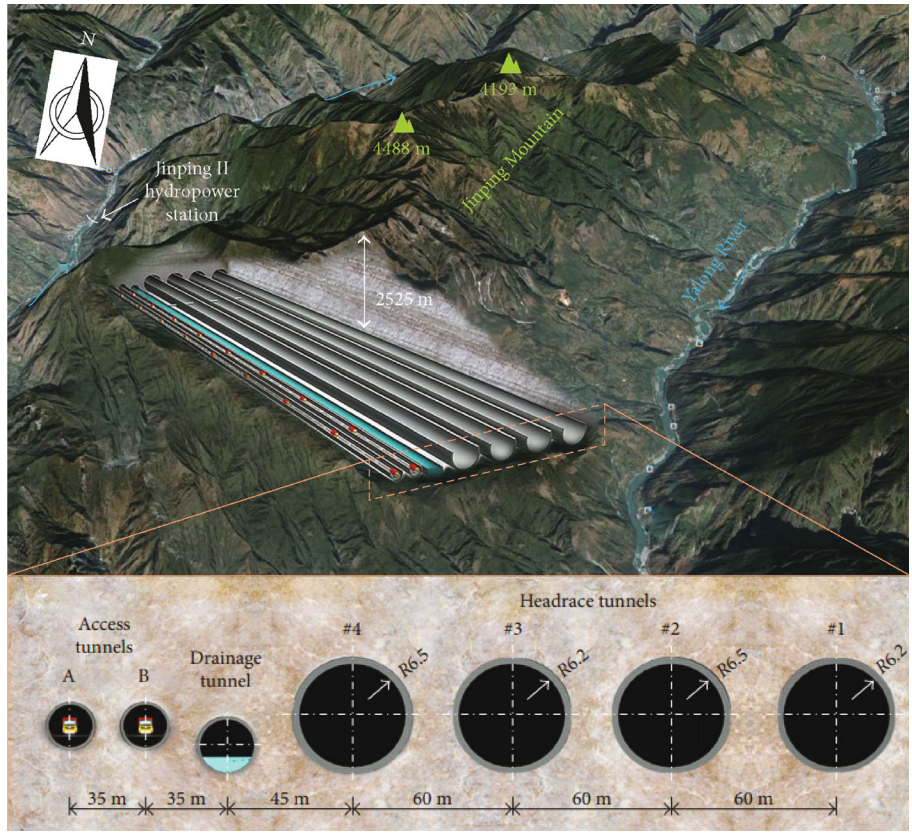

Figure 2: Layout and location of tunnels at the Jinping II hydropower station.

The above research results show that strain rockburst has three stages: splitting into plate, shearing into block, and ejection from block. However, there are still three shortcomings in this argument. (1) The syllogism of strain rockburst is drawn by analyzing the macroscopic failure phenomenon characteristics, dominant frequency characteristics, acoustic emission, and debris distribution law in the process of rockburst through special test paths, but the quantitative relationship of relevant parameters in the process of rockburst nucleation and failure is not given, which lacks of data support. (2) Due to the difficulty of the test and the limitation of the experimental conditions, small-scale and specific size rock samples are often used as a routine experimental study. However, as far as the large engineering scale is concerned, there is still a lack of in-depth discussion on the breeding mechanism and evolution process of the corresponding variant rockburst. (3) The relationship between the syllogism of strain rockburst and the prediction and early warning of rockburst is not revealed. Based on this, this paper taking Jinping deep-buried tunnel excavation as an example reveals the development process and failure mechanism of strain rockburst under unloading condition by studying the regularity of microseismic activity. Based on the evolution law of source parameters, the occurrence law and failure characteristics of deformation rockburst in three stages of incubation were studied, and then, the precursor information of microfracture of rock mass before rockburst was identified, and then, the internal relationship between deformation rockburst and microseismic was explored. After that, according to the response mechanism of each microseismic parameter variation to rockburst, real-time monitoring and early warning of tunnel strain rockburst can be realized.

Table 2: Physical and mechanical properties for Baishan group marble.

T_{2b} Baishan group marble	Value
Elastic modulus (GPa)	18.9
Poisson ratio	0.23
Friction angle ($/^{\circ}$)	25.8
Cohesion (MPa)	15.6
Weight (t/m^3)	27.5
Uniaxial compressive strength (MPa)	86

Table 3: Relationship between the parameters of sensors and the engineering scale.

Moment magnitude	-3	0	1
Sensor type	Accelerometer	Geophone	Geophone
Engineering scale	<300 m	<1 km	>2 km
Response frequency	10 kHz	500 Hz	200 Hz

Downloaded from http://pubs.geoscienceworld.org/gsa/lithosphere/article-pdf/doi/10.2113/2022/4135908/5676430/4135908.pdf
by guest

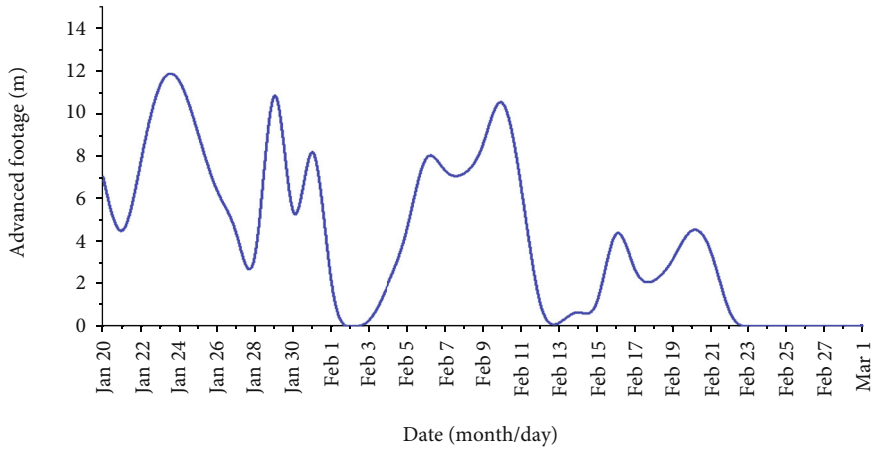

Figure 3: Daily advanced footage of TBM tunneling in diversion tunnel #3.

2. Microseismic Monitoring Technology, Scheme, and Results

2.1. Microseismic Monitoring Technology. In recent years, microseismic technology has been gradually used as an effective rockburst monitoring and warning method to ensure the safety and smooth construction of underground caverns. Tang et al. [17] introduced ESG microseismic monitoring system and discussed the feasibility of rockburst prediction based on the three elements of "space, time, and strength" of microseismic events and engineering cases. Feng et al. [1, 18–19] used ISS microseismic monitoring technology to analyze the generation mechanism, occurrence mechanism, and later dynamic support of rockburst in Jinping tunnel, and carried out research on the occurrence law, prediction, and early warning of rockburst, which achieved a lot of useful results. Ma et al. [20] based on the characteristics of rockburst precursor microseismic information carried out rockburst warning in deep tunnels under different construction conditions by means of microseismic monitoring and established tunnel rockburst prediction criteria. Feng et al. [21] proposed the rockburst risk warning technology with probabilistic quantification of rockburst level based on the microseismic monitoring technology and analyzed the rockburst cases in Jinping hydropower station. Based on the source model and microseismic event monitoring, Cai et al. [22] proposed a model of rock mass deterioration to quantitatively determine the position, quantity, and intensity of fractures. Zhao et al. [23] obtained a normal distribution relationship between the distribution of microseismic events in tunnels under engineering disturbances and the distance between working faces through the microseismic monitoring system. The spatial distribution characteristics of microseismic events are significantly spatially correlated with rockburst. Chen et al. [24] studied the cause and mechanism of instant rockburst and delayed rockburst through microseismic technology and analyzed the microseismic information precursors of two types of rockburst and applied them in tunnel rockburst warning. Based on the evolution law of microseismic activity, Xu et al. [25] found that the distribution of microseismic events had spatial consistency and time priority characteristics and took the event concentration degree as an important indicator before rockburst, and the results were applied to the prediction of tunnel rockburst.

The composition and monitoring process of the microseismic monitoring system are shown in Figure 1. The basic information of Jinping II hydropower station, such as engineering overview, geological conditions, monitoring principle, and microseismic monitoring network, has been introduced in detail in literatures [19–20, 25–27], which will not be repeated here. This paper focuses on the geological survey of the monitoring area, the selection of sensor parameters, and location methods of microseismic monitoring.

2.2. Monitoring Regional Geological Survey and Microseismic Monitoring Scheme. In the microseismic monitoring area, #3 diversion tunnel is located in the middle of the full-length tunnel segment in the lead (3) 8 + 000 ~ 11 + 000. The average buried depth is about 2212 m, and the maximum buried depth reaches 2525 m, which is the maximum buried depth of the full-length tunnel line (see Figure 2 for details). This area is mainly the gravity field, and the maximum principal stress is 71 MPa, which is the maximum in situ stress of #3 diversion tunnel. In this area, the karst and groundwater are not developed in the project area, and the lithology is T_{2b} gray to gray white dense and thick bedded crystalline limestone and marble. The surrounding rock is mainly type II-III, with good integrity and no large fault zone. The physical and mechanical parameters of typical rock layer are shown in Table 2. The rock is hard and brittle, and the uniaxial compressive strength is between 90 and 100 MPa under dry conditions. The measured rockburst tendency index (W_{et}) of rock mass ranges from 1.32 to 5.8, reflecting that the rock along the axis of the cave has high energy storage property and the strength condition of high in situ stress failure. Therefore, the lithology of this section has the properties of high buried depth, high in situ stress, high energy storage, and good integrity. According to the occurrence conditions and characteristics of strain rockburst, the tunnel section has sufficient conditions for strain rockburst.

Downloaded from http://pubs.geoscienceworld.org/gsa/lithosphere/article-pdf/doi/10.2113/2022/4135908/5676430/4135908.pdf
by guest

There are two types of sensors, i.e., geophone and accelerometer, for microseismic monitoring. The main difference between the two types of sensors is the monitoring frequency response (the response frequency range of geophones is relatively low). Table 3 summarized the relationship between the sensor type, moment magnitude scale, response frequency, and engineering scale. The maximum diameter of the excavation section of the diversion tunnel of Jinping II hydropower station is 13 m, so the influence distance of the excavation section should be within 100 m in front of the working face. The area within 300 m behind the excavation section needs to be monitored, and the engineering scale of the excavation of the diversion tunnel of Jinping II hydropower station is about 400 m, so the acceleration sensor was selected. The sensitivity of the sensor is 30 V/g, and the frequency response is 50 Hz to 5 kHz. The selection of sensor types are shown in Table 3.

Many positioning algorithms are available, including the Geiger location method, the master-event relative relocation method, the double-difference relocation method, the simplex location method, and the least-squares location method. The Geiger location method was used in this study to localize the microseismic events, and its specific purpose was to converge on a final result from a given initial point (test point) via iteration. Based on the least-squares method, a corrected vector $\Delta\theta$ (Δx, Δy, Δz, and Δt) calculated in each iteration was added to the result (test point) from the previous iteration to obtain a new test point. Then, the new test point was assessed to determine whether it met the necessary requirements. If so, the coordinates of the point were considered to represent the hypocentral location of the event; otherwise, iteration was continued. The result of each iteration was generated using the time-distance equation. A homogeneous velocity model was used in the system for calculating the parameters of microseismic events, and the results were recorded the data to a hard disk. It is worth [1]noting that constant *P*- and *S*-wave velocities were initially estimated from artificial blasting tests and used to calculate event locations. The calibration results indicated velocities of $V_p = 2800$ m/s and $V_s = 1800$ m/s.

2.3. Microseismic Monitoring Results. The daily excavation length of the tunnel is shown in Figure 3. From January 20 to February 5, 2011, the spatial and temporal intensity distribution of microseismic time is shown in Figure 4(a). In this period, 192 microseismic events were generated. Although the number of microseismic events was large, the distribution was discrete without clustering area, and low-energy small earthquakes dominated, so the risk of rockburst was low. From February 6 to 11, more microseismic events were generated and accelerated to gather on the north side wall 25 m behind the working face and then forming a zonal microseismic event cluster (blue area in the figure). On February 10, the number of microearthquakes was up to 22, and there were 5 events larger than 3500 J, with a maximum of 1.69×10^4 J. The energy released by surrounding rock was much higher than the release level of the previous days. It implies that large-scale fractures occurred within the surrounding rock mass, and the rockburst risk was high.

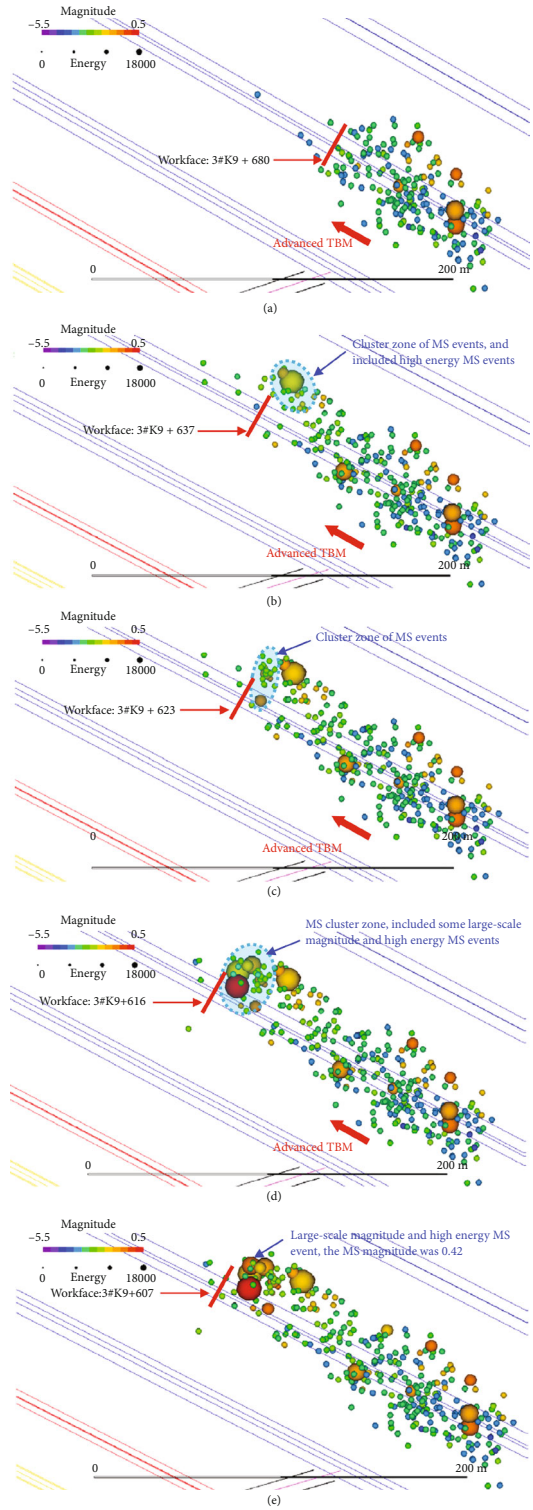

Figure 4: A projection map of the spatio-temporal distribution of microseismicity during TBM tunneling in diversion tunnel #3 (January 20 to February 21, 2011). (a) Distribution of microseismic events from Jan. 20 to Feb. 5, 2011. (b) Distribution of microseismic events from Jan. 20 to Feb. 11, 2011. (c) Distribution of microseismic events from Jan. 20 to Feb. 16, 2011. (d) Distribution of microseismic events from Jan. 20 to Feb. 19, 2011. (e) Distribution of microseismic events from Jan. 20 to Feb. 21, 2011.

Downloaded from http://pubs.geoscienceworld.org/gsa/lithosphere/article-pdf/doi/10.2113/2022/4135908/5676430/4135908.pdf
by guest

Table 4: On-site records of strain rockbursts within the tunnel section of 3# K9 + 770 ~ K9 + 607.

Rockburst time	Rockburst location	Rockburst type	Level of rockburst	Representation form
2.11 03:30	9 + 637 ~ 675	Strain	Intense	Plate-like splitting, stratified peeling, accompanied by a crisp burst sound.
2.13 18:11	9 + 651 ~ 652	Strain	Slight	Peel off, slice to help, give priority to with fragmentary piece.
2.16 21:57	9 + 623	Strain	Medium	T_{2b} marble type III surrounding rock, slab wall, ejecting, a large number of wedge fragments, the crater is v-shaped, partial collapse, and slight rock burst occurred before rock burst.
2.16 22:00	9 + 628 ~ 633	Strain	Intense	
2.16 23:40	9 + 628 ~ 635	Strain	Intense	
2.18 14:50	9 + 627	Strain	Medium	To split or eject into wedge-shaped fragments.
2.18 19:10	9 + 626	Strain	Medium	
2.19 15:42	9 + 621 ~ 626	Strain	Intense	A large number of wedge fragments ejection, splitting, before the occurrence of a crisp cracking sound, "V" shaped crater.
2.21 5:45	9 + 607 ~ 626	Strain	Extremely intense	A large number of fragments were ejected and accompanied by large pieces of rubble which caused several landslides behind the face of the palm.
	9 + 613 ~ 618	Strain	Extremely intense	
	9 + 651 ~ 664	Strain	Slight	

From February 12 to February 16, there were concentrated signs of microseismic activity in the north side wall ~ arch shoulder of (3)9 + 629 ~ 639. There were 13 microearthquakes in total on February 16, of which 5 events were larger than 5000 J, with a maximum of 1.41×10^4 J. The energy loss of surrounding rock was larger than that of the earlier stage. From February 17 to 19, the cluster of microseismic activity continued in the north side wall to the shoulder, and the cluster range gradually expanded, forming a concentrated area of microseismic activity in the working face 9 + 607 to 9 + 622. In this period, although there were few microseismic events, there were many high energy and large magnitude microseismic events, events larger than 5000 J accounted for 29.6% of the total, and the maximum energy release was 5.32×10^4 J. The occurrence of a large number of high-energy microseismic events indicates that some large-scale fractures occurred induced by the excavation unloading, and the stability of the surrounding rock mass decreased. From February 20 to February 21, there were 12 microseismic events. Although there were less than 2 large microseismic events with high magnitude and energy, the maximum magnitude was as high as moment magnitude = 0.509, and the maximum energy was as high as 1.16×10^4 J.

3. Nucleation Mechanism and Process of Strain Rockburst

3.1. Occurrence Characteristics of Strain Rockburst. During TBM tunneling, strain rockburst occurred 11 times successively from 9 + 600 to 9 + 800. There were 2 slight rockbursts, 3 moderate rockbursts, 3 intense rockbursts, and 3 extremely intense, respectively. On the whole, rockburst occurred most frequently and intensely from February 16 to February 19. On February 21, the damage range was the largest and strongest, and the cumulative damage length was 37 m. The occurrence and failure characteristics of strain rockburst are shown in Table 4.

The first strain rockburst occurred on February 11, 2011. An intense rockburst occurred 7 m~45 m behind the working face. The length of rockburst damage was 38 m, and the damage was accompanied by a clear burst sound; the on-site rockburst is shown in Figure 5(a). It can be seen that the failure location is mainly concentrated in the north side wall to the shoulder, and the main failure mode is plate splitting and stratified spalling. The fracture surface is parallel to the side wall, and the depth of the explosion pit is 0.1 m~0.5 m. Then, on February 13, a slight rockburst occurred between 9 + 651 and 652. The rockburst occurred in a small scale and concentrated on the north side wall, in the form of thin plate splitting, splintering, and sporadic fragments.

On February 16, a medium rockburst occurred in the working face (3)9 + 623 and two intense rockbursts occurred in the range of 5 m~12 m behind the working face. The cumulative damage length of the three rockbursts was about 13 m. These rockbursts were accompanied by continuous loud blast-like sounds; the on-site rockburst is shown in Figure 5(b). It can be seen that the damage location is in the south and north side of the wall and the arch to vault area. The main form of destruction is a large number of wedge-shaped fragmentation projectile phenomenon. The typical pits are V-shaped and larger in size, with depths ranging from 0.1 m to 0.6 m. On February 18, two moderate rockbursts occurred in the range of 7 m~8 m behind the working face. The damage location is mainly concentrated on the south side wall and arch shoulder, and the damage form is mainly a small amount of splitting and wedge fragments ejection. Then, on February 19, an intense rockburst occurred from 9 + 621 to 626, accompanied by muffled sound. The length of rockburst was 5 m, and the damage location was from the north side wall to the vault. The crater was V-shaped with a depth of about 0.3 m.

The most severe strain rockburst with the largest impact area occurred at 5:45 on February 21. Two extremely intense rockbursts occurred in the 0~19 m and 6~11 m holes behind

Downloaded from http://pubs.geoscienceworld.org/gsa/lithosphere/article-pdf/doi/10.2113/2022/4135908/5676430/4135908.pdf
by guest

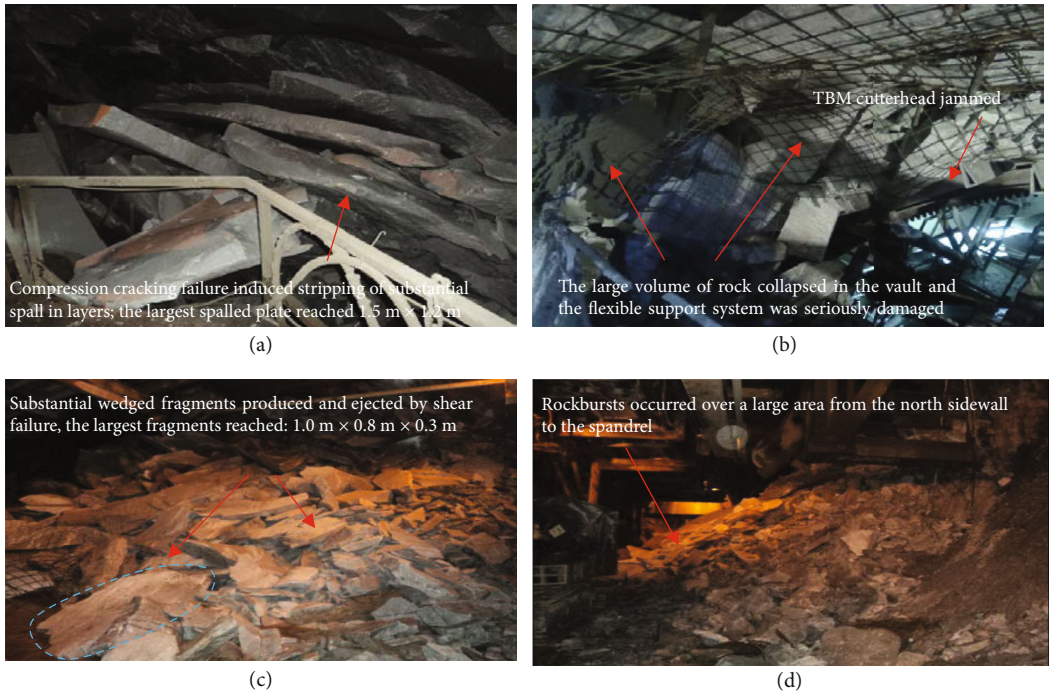

Figure 5: On-site photos showing the failure caused by stainrockburst. (a) Spalling caused by compression-induced tensile damage. (b) Damage of shotcrete and flexible support system. (c, d) A large area of damaged rockmass occurred along the tunnel axis, a large number of blasting blocks fell across the south and north side walls, and the tunnel collapsed in an all-round way.

9 + 607 at the working face, which were the most violent and destructive events among the 11 events (Figures 5(c) and 5(d)). At the same time, there was also a slight rockburst at the location of 44 m~57 m behind the working face, with a cumulative rockburst length of 37 m. The damage occurred on the north and south side of the wall ~ vault. The main failure mode is blasting block ejection accompanied by plate splitting. The rockburst caused the anchor bolt to fall off, the steel net to be destroyed, the TBM cutter head to be stuck, and caused several collapses behind the face of the face, and the support system was seriously damaged. The maximum blasting block can reach 1.0 m × 0.8 m, the maximum blasting pit depth is 1.2 m, and the blasting block ejection distance is 1 m~4 m. The tunnel was instantly filled with gray dust with very loud sounds.

3.2. Failure Mechanism Analysis of Strain Rockburst. In seismology, the energy ratio of shear wave S to compression wave P, i.e., E_S/E_P, is an important parameter reflecting earthquake focal mechanism [28]. Gibowicz et al. and. Krajcinovic and Silva [28, 29] found that fault-slip type or shear type failure occurred if $E_s/E_p \geq 10$ when they studied the law of energy release of relevant seismic waves. When $E_s/E_p \leq 3$, it is related to the nonshear failure such as strain rockburst, stress, or volume-induced seismic events [30]. When $3 < E_s/E_p < 10$, the tensile failure occurred. Figure 6 shows the distribution characteristics of the ratio frequency of microseismic events in the monitored cavern during the rockburst period [31]. From February 1 to February 21, 2011, the E_s/E_p were mainly distributed in the range of 0 to

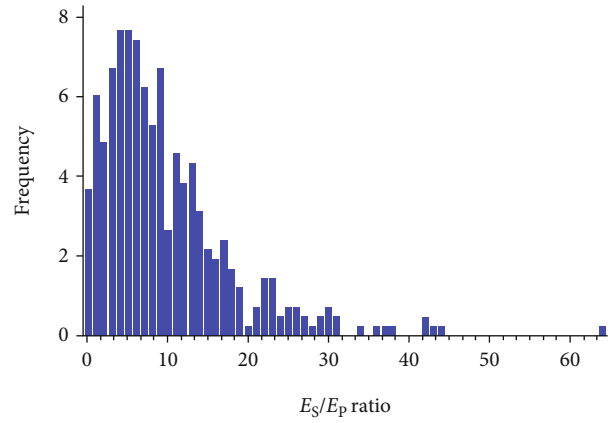

Figure 6: Frequency distribution of E_S/E_P at #3 underground tunnel.

44, accounting for 99.7% of the total. Among them, the microseismic events of $E_s/E_p < 10$ accounted for 72.1% of the total. However, the microseismic events of $E_s/E_p \geq 10$ accounted for 27.9% of the total. The results show that the damage and failure of rock mass of tunnel is mainly caused by tensile failure, accompanied by a large number of shear failure.

3.3. Nucleation and Development Process of Strain Rockburst. In general, there are two clusters of microseismic events in tunnel diversion section (3)9 + 600 – 9 + 700, corresponding

Downloaded from http://pubs.geoscienceworld.org/gsa/lithosphere/article-pdf/doi/10.2113/2022/4135908/5676430/4135908.pdf
by guest

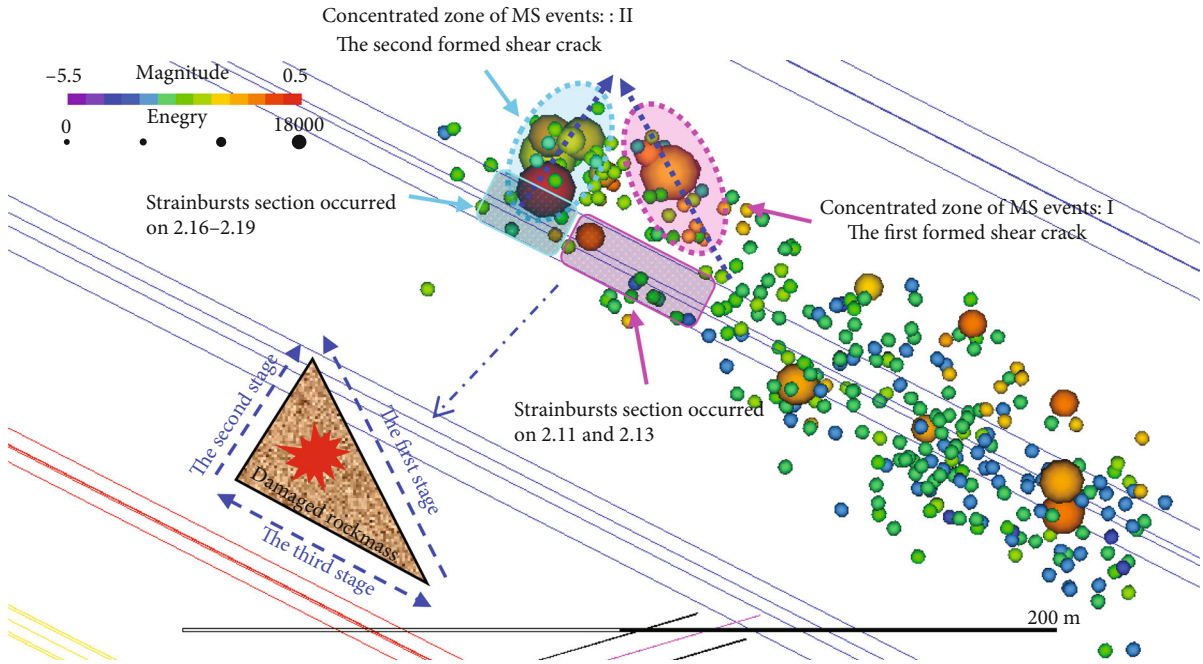

Figure 7: Evolution of rockburst nucleation process during TBM tunneling in diversion tunnel #3.

to tunnel diversion section (3)9 + 640 − 662 and tunnel diversion section (3)9 + 607 − 637, as shown in Figure 7. During this period, according to the spatial and temporal distribution characteristics of microseismic activity, rockburst occurrence time, location, and intensity, failure mode and mechanism, and the evolution characteristics of microseismic parameters, the initiation and development process of strain rockburst can be divided into three stages.

The first one is the initiation and development stage of tensile crack (Feb. 5~Feb. 11). At this stage, the surrounding rock was first caused by compression-induced tensile failure at the shallow surface of the tunnel, and a large number of thin plates are split and obvious plate cracking occurs due to the compression-induced tensile failure (Figure 5(a)). With the continuous construction disturbance and failure, the underground stress field was redistributed and transferred, which leads to the further extension of rock fissures to the depth of the tunnel and then leads to the strip-like distribution of microseismic activity intensive area I (blue ellipse, namely, shear zone I). At this stage, the extension of the tensile crack is deep, so the shear crack may be formed rapidly in the later stage, which leads to the occurrence of local rockburst. The failure process at this stage is consistent with the view of Zhou et al. [32–33] that there is an intense correlation between plate cracking and rockburst, that is, plate cracking is a precursor characteristic of rockburst. In this stage, the failure mode is mainly split and delamination of thin plate. Among them, $3 < E_s/E_p < 10$ and $E_s/E_p \geq 10$ accounted for 63.5% and 26.6% of the total, respectively, indicating that the rock mass damage and failure of tunnel is mainly tensile failure, accompanied by a large number of shear failure. In the first half of failure, the tensile is the main failure, while shear failure is the main one in the fracture far from the surface, and tensile crack appears earlier than shear crack.

The second one is the macroscopic shear crack formation stage (Feb. 12-Feb. 19). When the tensile cracks grow to a certain extent, oblique shear cracks will inevitably occur, and then, macroscopic shear cracks will be formed. In this stage, the microseismic events gather along the dense area II (pink ellipse, namely, shear zone II), and the number of microseismic events formed by the mixed failure of microfracture stretching and tensile shear increases rapidly in the later stage. As the working face advances, high-energy and large magnitude events continue to occur in the region, indicating that macroshear cracks are gradually developing in the region. Compared with the intense rockburst in the first stage, the damage degree of this rock mass is more severe and serious in terms of moment magnitude and energy loss, which is the most severe stage of rockburst occurrence and destruction. A total of 26 microseismic events were larger than 5000 J, and the maximum one-day energy release reached 6.89×10^4 J. In addition, the failure modes of this stage are mainly V-shaped blasting pits and stepped structural plane fracture. Similar to the first stage, tensile failure accounted for 57.7% of the total, indicating that the tunnel failure was still mainly tensile failure, but the increase of shear ratio accounted for 35.4% of the total. This stage is the most frequent and violent rockburst, which belongs to the main shock stage of rockburst.

The third one is the overall instability stage (Feb. 20~Feb. 21). As the shear cracks generated in the two stages are connected with each other, a triangular region is formed with the cave-wall surface. In addition, the ground stress in this area is high, and the main earthquake and main failure have been completed in the first two stages, so the rock mass

Downloaded from http://pubs.geoscienceworld.org/gsa/lithosphere/article-pdf/doi/10.2113/2022/4135908/5676430/4135908.pdf
by guest

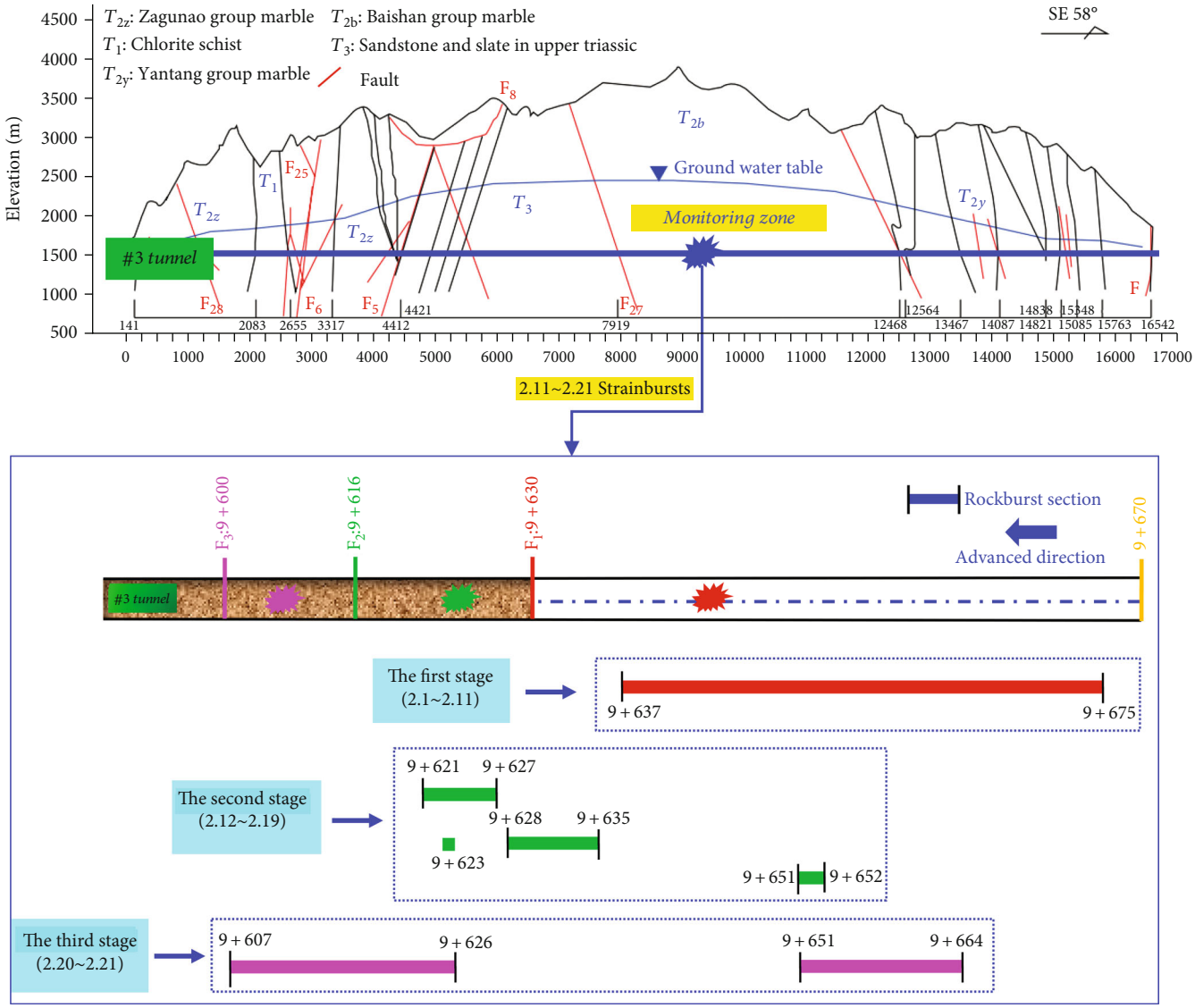

Figure 8: Schematic diagram of specific location and scope of strain rockburst.

is unstable as a whole in this stage, accompanied by a larger rockburst. The cumulative length of rockburst is 37 m, and a slight rockburst occurs 35 m away from the rear of the working face. Different from the first two stages, this stage of $E_s/E_p < 10$ accounts for 96.6% of the total, indicating that the instability failure in this stage is mainly tensile failure.

To sum up the above three stages of failure, although dozens of rockbursts with mild to strong intensity occurred successively from Feb. 11 to Feb. 21, it can be considered that the failure process of a complete strain rockburst is caused by multiple rockbursts from the overall failure time, relative spatial position, failure process, failure mode, and severity. It is completed by combination of stages (different time and location) and fractional intensity (slight ~ extremely intense rockburst). The relative spatial location and time of failure are shown in Figure 8 and Table 5. In the first stage of sheet stripping, the failure of rockburst is mainly tensile failure, manifested in the form of sheet cracking and stratified stripping, which is the precursor feature of intense rockburst, and the crack growth belongs to the steady state expansion stage. The rockburst in the second stage is the main failure stage. In this stage, the shear failure increased obviously, the damage of rock mass is the first stage which is more serious, and the stage of rockburst occurred in the short time interval, high frequency, and severe. Therefore, the microcracks by steady-state extension development become unsteady rapidly expanded, and in the extension process accompanied by a large number of elastic strain energy release. In the process of comprehensive collapse, the stress and energy transfer and release to the tunnel surface after the two shear bands are interconnected, accompanied by a large number of block throwing and ejection phenomenon, resulting in the instability failure of the tunnel wall in a large area. These three stages of rockburst failure process are in good agreement with the

Downloaded from http://pubs.geoscienceworld.org/gsa/lithosphere/article-pdf/doi/10.2113/2022/4135908/5676430/4135908.pdf
by guest

Table 5: Expression forms and failure characteristics of strain rockburst in different development stages.

	The first stage	The second stage	The third stage
Failure mechanism	Tensile failure is the main failure, accompanied by a large number of shear failure, accounting for 63.5% and 26.6%, respectively.	Tensile failure was the main failure, but shear failure increased significantly, accounting for 57.7% and 35.4%, respectively.	Tensile failure, 96.6% of the failure
Crack propagation state	Stable crack growth	Unstable crack growth	Stable crack growth
Motion characteristics of blasting block	A plate-shaped layered peeling, no initial speed	To throw or eject, with a certain initial speed and range	To throw or eject, with a certain initial speed and range
Failure mode	A large number of vertical plate cracking, layered peeling	A large number of wedge-shaped fragments were catapulted, burst, and loose, and a small number of plates were split. The size of the crater was large, with a depth of 0.1 m~0.6 m, which was typical "V" type	A large number of wedge-shaped fragments were ejected and accompanied by large pieces of rubble which caused several landslides behind the face of the palm.
Degree and intensity of damage	Intense (1 intense rockburst), foreshock stage.	Main failure stage, this stage is the most violent destruction, rockburst frequency (higher slight rockbursts 6 times), belongs to the main shock stage	Severe, the tunnel completely unstable collapse (extremely strong rockbursts 2), aftershock stage.
Cumulative failure length	38 m	20 m	32 m

rockburst failure process and research results of true triaxial unloading test of rock in literature [8–10, 15–16].

4. Microseismic Activity Characteristics of Strain Rockburst Nucleation Process

4.1. Variation Characteristics of Microseismic Energy. The microseismic energy loss per unit time is closely related to the strength and damage degree of rock mass, which reflects the continuous development of microdefects in rock and the process of strength weakening and eventually losing. The corresponding relationship between microseismic energy and time in no. 3 diversion tunnel from February 1 to March 1, 2011, is shown in Figure 9. The three peaks of microseismic energy loss (2.10, 2.19, and 2.21, respectively) exactly correspond to the three stages of rockburst failure, indicating that a large amount of energy is released before each stage of rockburst failure. Before each intense rock burst, the energy released by microfracture of rock mass shows an upward trend, and the cumulative energy released has the characteristics of sharp increase and sudden increase. Especially in the second stage of rockburst, the cumulative release energy of microseismic is the most significant, and the single-day peak energy reaches 6.89×10^4 J. This phenomenon belongs to the typical abnormal microseismic activity, and the rockburst signs are obvious.

4.2. Characteristics of Moment Magnitude Variation of Microearthquakes. According to the distribution relationship between the magnitude and time of microseismic (seen in Figure 10), corresponding to the failure process of rockburst, the concentrated release of the moment magnitude is also obviously divided into three stages. The moment magnitude of microseismic will gradually rise with the progress of rockburst failure. The failure intensity and failure form of the three stages are also different, and the average magnitude reaches the maximum in the third stage. Minor events with magnitudes lower than 0 accounted for the majority, and major events with magnitudes higher than 0 accounted for 15. The largest number of large earthquakes and their intensity mainly occurred from February 16 to February 19 in the second stage. The number of microseismic events with moment magnitude ≥ 0 was 11, accounting for 73.3% of the total number of large magnitude, and the maximum moment magnitude reached 0.547. After the completion of the main failure (main shock) stage of the second stage rockburst, the high magnitude events of the third stage are obviously reduced. Compared with the first stage, the damage degree of rock mass in the second stage is more severe and severe, the crack growth rate is faster, the release level and intensity of elastic strain energy are greater, and the damage of rockburst is more severe.

4.3. Variation Characteristics of Apparent Microseismic Volume and Energy Index. In seismological theoretical research, apparent stress, apparent volume, and energy index are important physical quantities used to describe earthquake nucleation and development [34]. These statistical parameters of microseismic activity reflect the evolution law and change characteristics of the surrounding rock mass before the earthquake and have been widely used to evaluate the stability of a rock mass [35].

According to the typical stress-strain curve of rock, the deformation growth is accelerated, and the stress growth is slow when the rock is close to the peak strength. In the late peak period, the stress decreases with the increase of deformation. When the rock mass is in the strain-softening stage, the larger the stress drop, the greater possibility of rock mass instability, and the more serious the failure degree [36, 37]. Therefore, the slope of cumulative apparent volume $\sum V_A$

Downloaded from http://pubs.geoscienceworld.org/gsa/lithosphere/article-pdf/doi/10.2113/2022/4135908/5676430/4135908.pdf
by guest

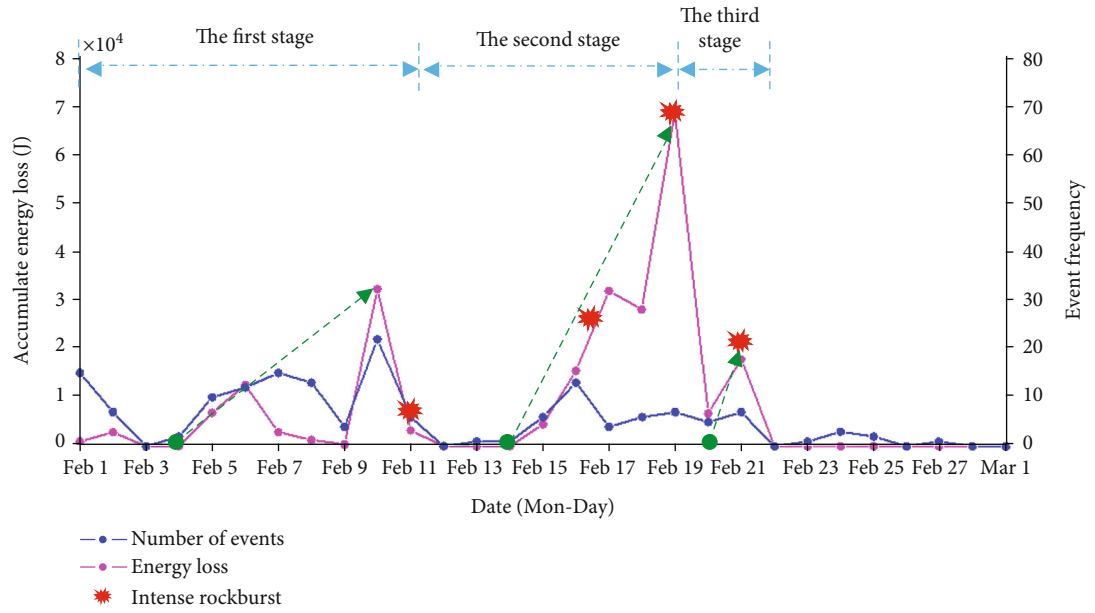

Figure 9: Correlation chart between microseismic energy, microseismic activity rate, and time.

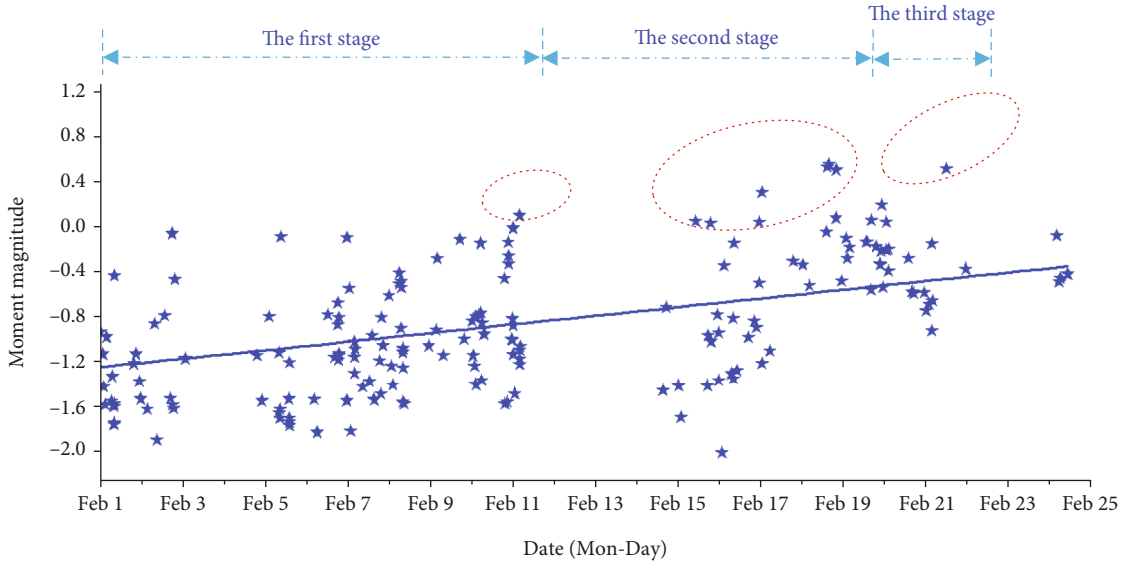

Figure 10: The relationship between magnitude distribution and time in #3 diversion tunnel.

over time is often regarded as an important indicator of rock strain rate. The expressions of apparent stress and apparent volume are [38]:

$$\sigma_A = \frac{E}{P}, \tag{1}$$

where E is the seismic energy and P is the seismic potential.

$$V_A = \frac{\mu P^2}{E} = \frac{M}{2\sigma_A}, \tag{2}$$

where E is the seismic energy; μ is shear stiffness; M is seismic moment; and σ_A is depending on the stress.

The energy index refers to the ratio of the radiation energy generated by the seismic event to the average seismic energy $\bar{E}(P)$ of all seismic events in the same monitoring area [38]. The average seismic energy can be obtained from the relation $\log \bar{E}(P) = c_1 \log P + c_2$, where P represents seismic potential. c_1 and c_2 are constant.

$$EI = \frac{E}{\bar{E}(P)} = \frac{E}{10^{c_1 \log P + c_2}} = 10^{-c_2} \frac{E}{P^{C_1}}. \tag{3}$$

The energy index reflects the variation of driving stress in the source region. According to the instability theory of rock, strain softening occurs in the later stage of rock failure,

Downloaded from http://pubs.geoscienceworld.org/gsa/lithosphere/article-pdf/doi/10.2113/2022/4135908/5676430/4135908.pdf
by guest

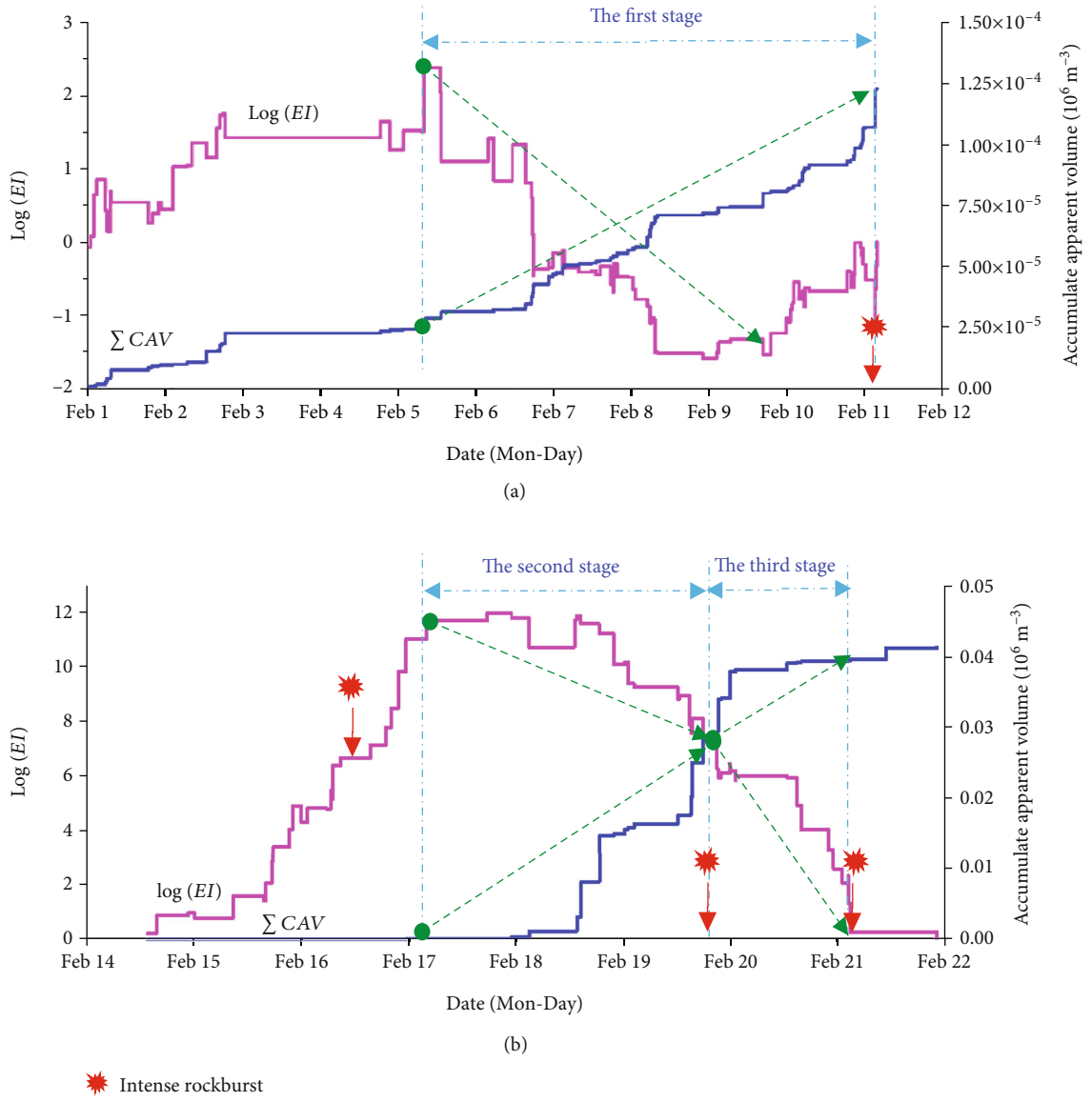

FIGURE 11: Time history plot of relationship between energy index and accumulate apparent volume in the #3 diversion tunnel. (a) Curves of energy index and cumulative apparent volume over time from 1 February to 11 February. (b) Curve of energy index and cumulative apparent volume over time from Feb. 14 to Feb. 22.

and the larger the stress drop is, the more serious the rock damage is. Therefore, the greater the energy index in a monitoring area, the higher the stress level in the area. The rapid decrease of energy index indicates that the instability of rock mass increases, and the probability of big events increases greatly.

Figures 11(a) and 11(b) clearly show that at each stage of strain rockburst development, the energy index and cumulative apparent volume show abnormal fluctuations, that is, the energy index decreases rapidly, and the cumulative apparent volume increases rapidly. Therefore, there are too many data missing between 2.12 and 2.14. The data in this period cannot be available in the figure. In particular, from February 18 to February 21, the cumulative apparent volume increased rapidly, and the energy index decreased significantly twice after reaching the peak value on February 18 and finally dropped to the lowest value. According to the physical significance of cumulative apparent volume and energy index, it indicates that the driving stress of surrounding rock has released a large number of energy and experienced the compaction stage and elastic stage before the peak strength, and the rock mass has entered the strain softening stage, which is the precursor feature before the occurrence of rockburst. In addition, from the comparison of the two figures, it is found that in terms of the order of magnitude of cumulative apparent volume and energy index, Figure 11(b) fluctuates more than Figure 11(a), and the downward slope of energy index is also larger. It reflects that the second and third stages of rockburst incubation process are more violent than the first stage, and the precursory characteristics are more obvious.

Downloaded from http://pubs.geoscienceworld.org/gsa/lithosphere/article-pdf/doi/10.2113/2022/4135908/5676430/4135908.pdf
by guest

Table 6: Details of the b value from Jan 30, 2011, to Feb 21, 2011.

Sequence number of events	Occurrence time of corresponding events	b value	Remarks
1-30	Jan 30, 2011—Jan 30, 2011	1.093	
16-45	Jan 31, 2011—1 Feb, 2011	1.258	
31-60	1 Feb, 2011—5 Feb, 2011	0.91	
46-75	2 Feb, 2011—6 Feb, 2011	0.782	
61-90	5 Feb, 2011—7 Feb, 2011	0.835	
76-105	6 Feb, 2011—8 Feb, 2011	0.958	
91-120	7 Feb, 2011—10 Feb, 2011	1.008	
106-135	8 Feb, 2011—10 Feb, 2011	0.747	"2.11" rockburst
121-150	10 Feb, 2011—15 Feb, 2011	0.682	
136-165	10 Feb, 2011—16 Feb, 2011	0.635	"2.16" rockbursts
151-180	15 Feb, 2011—19 Feb, 2011	0.517	"2.18" and "2.19" rockbursts
166-195	16 Feb, 2011—20 Feb, 2011	0.781	"2.21" rockbursts
181-206	19 Feb, 2011—21 Feb, 2011	1.109	

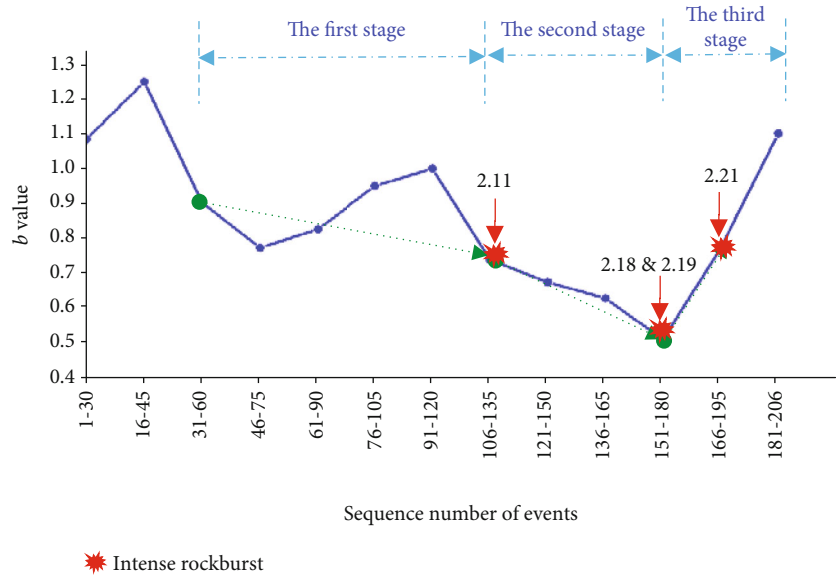

Figure 12: Change of b value and time in the #3 diversion tunnel.

4.4. The Variation Characteristics of b Value. Existing research results show that both microseismic events induced by engineering disturbance and natural seismic events follow the magnitude-frequency (G-R) relationship, which was obtained by Gutenberg and Richter [39] after statistics. The formula can be expressed as:

$$\lg N(M) = a - bM, \tag{4}$$

where M is the magnitude of rockburst; $N(M)$ is the total number of microseismic events with magnitude above M; a and b are constants for a given monitoring region.

As an effective parameter commonly used in seismological analysis of magnitude-frequency, b value represents the proportional relationship between the number of large magnitude and the number of low magnitude in a certain region. When the value of b increases, it indicates that the number of events of large magnitude is less, and the number of small magnitude is more. When the value of b decreases, it indicates that the proportion of high magnitude events increases, and the stability of rock mass begins to decline. Therefore, the change of b value is closely related to the damage of rock mass and the disasters caused by it, and the development process of rockburst can be analyzed by using the change law of b value.

In order to avoid the large fluctuation and error of b value due to the large difference in the number of microseismic events generated every day, the number of events in the selection range is too much or too little. A moving window method was adopted for the calculation of the b value [40] in this study, and 30 events and 15 events were used for the estimating window and sliding window, respectively. Table 6 and Figure 12 show the change of b value over time from January 30, 2011, to February 21, 2011. It can be seen

Downloaded from http://pubs.geoscienceworld.org/gsa/lithosphere/article-pdf/doi/10.2113/2022/4135908/5676430/4135908.pdf
by guest

from the figure that when the rock mass is stable without failure, the b value fluctuates higher 0.91. In the first stage, the value of b decreased to 0.747~1.008 and reached the minimum value of 0.747 especially before the rockburst on 2.11. However, in the second stage, b value drops rapidly and at a relatively low level, finally falling to 0.517, which is also the most intense stage of rockburst. In the third stage, b value rose slightly to 0.781 because the main shock and main failure stage had been completed in the second stage, and the surrounding rock was in the instability failure stage after the cracks were interconnected. The above changes in b values indicate that the number of large seismic events in rock mass begins to increase, and the proportion of large-scale microcracks in the total number begins to increase. After the integration and connection of small-scale cracks, large-scale cracks form. The spatial distribution of microcracks in rock mass changes from disorderly distribution to ordered self-organization, which is a significant feature in the process of rockburst incubation. In conclusion, the rapid decline of b value in a certain period of time can be considered as the microfracture precursor of rockburst disaster.

To sum up, the incubation and development process of strain rockburst is the gradual transformation from static equilibrium to dynamic instability of rock mass, which can be reflected in the three stages of rockburst incubation and failure. In this process, the microseismic parameters vary in different degrees. According to the statistical parameter variation characteristics of rockburst macrodamage intensity and microseismic activity, there are essential differences in each stage of rockburst incubation process. Therefore, it is of great engineering value and reference significance to distinguish the failure characteristics in different stages of rockburst nucleation by the fluctuation law of source parameters and adopt different support means and measures in time for the prediction and early warning of strain rockburst.

5. Conclusions

This paper takes the rockburst section of #3 diversion tunnel of Jinping Hydropower Project as an example, based on microseismic event of the "time, space, and intensity" distribution characteristics, and law of seismic activity research, nucleation and nucleation process of strain rockburst, and macroeconomic instability failure mechanism are revealed under the condition of excavation unloading, the gradual damage process of rockburst is studied in different stages of the corresponding failure mode and failure characteristics and explores the microtremor evolution law and the internal relations between rockburst, and the main conclusions are as follows:

(1) The nucleation and development process of strain rockburst under engineering excavation can be divided into three stages: tensile crack initiation and development stage, macroshear crack formation stage, and overall instability stage. The failure process of rock mass of the superficial, the microcrack initiation, extended to the macroscopic shear crack is formed after the deep rock mass has formed two macroscopic shear cracks with free face to form a closed triangular area; the area of rock mass in slab split, layered peeling, v-shaped blasting hole, the phenomenon such as rock throwing ejection, eventually lead to intense rockburst and overall collapse. The rockburst failure process under engineering excavation is in good agreement with the rockburst syllogism. Compared with other rockburst mechanism studies, the progressive failure view of strain rockburst in this paper can explain the nucleation mechanism better

(2) Different stages of strain rockburst nucleation correspond to different macrofailure characteristics and microseismic evolution characteristics. The abnormal clustering of microseismic event, the increase of high energy and large magnitude events, the continuous and rapid increase of microseismic energy and cumulative apparent volume, and the rapid decrease of energy index and b value are positively correlated with the intensity of rockburst. Based on the above study on the timing sequence variation and fluctuation characteristics of source parameters, it can effectively serve as the precursor characteristics and early warning indicators of strain rockburst failure and provide reference for rockburst monitoring and early warning of similar deep tunnel engineering

Data Availability

The research data in this paper was taken from the rockburst section in the deep-buried tunnel of the Jinping II Hydropower Project of Yalong River, Sichuan Province, China.

Conflicts of Interest

The authors declare no conflicts of interest.

Acknowledgments

This study was supported by the Social Governance Science and Technology Special Project of Shenyang (20-206-4-11), Science and Technology Project of Transportation Department of Liaoning Province (2021034), and National Natural Science Foundation of China (grant no. 52179123).

References

[1] X. T. Feng, B. R. Chen, C. Q. Zhang, S. J. Li, and S. Y. Wu, *Mechanism Warning and Dynamic Control of Rockburst Development Processes*, Science Press, Beijing, China, 2013.

[2] P. K. Kaiser and M. Cai, "Design of rock support system under rockburst condition," *Journal of Rock Mechanics and Geotechnical Engineering*, vol. 4, no. 3, pp. 215–227, 2012.

[3] C. S. Zhang, N. Liu, W. J. Chu, and S. H. Ni, "Inducement mechanism and case analysis of tectonic rockburst in Jinping II deep buried tunnel," *Chinese Journal of Rock Mechanics and Engineering*, vol. 34, no. 11, pp. 2242–2250, 2015.

Downloaded from http://pubs.geoscienceworld.org/gsa/lithosphere/article-pdf/doi/10.2113/2022/4135908/5676430/4135908.pdf
by guest

[4] S. Y. Wu, Q. M. Gong, G. Wang, Z. S. Hou, and Q. R. She, "Experimental study of slabbing failure for deep-buried marble at Jinping II hydropower station and its influences on TBM excavation," *Chinese Journal of Rock Mechanics and Engineering*, vol. 29, no. 6, pp. 1089–1095, 2010.

[5] S. F. Wang, L. C. Sun, X. B. Li et al., "Experimental investigation and theoretical analysis of indentations on cuboid hard rock using a conical pick under uniaxial lateral stress," *Geomechanics and Geophysics for Geo-Energy and Geo-Resources*, vol. 8, no. 1, pp. 1–23, 2022.

[6] Y. A. Tan, "Analysis of fractured face of rockburst with scanning electron microscope and its progressive failure process," *Journal of Chinese Electron Microscopy Society*, vol. 2, pp. 41–48, 2010.

[7] M. C. Gu, F. L. He, and C. Z. Chen, "Study on rockburst in Qingling tunnel," *Chinese Journal of Rock Mechanics and Engineering*, vol. 21, no. 9, pp. 1324–1329, 2002.

[8] M. C. He, J. L. Miao, D. J. Li, and C. G. Wang, "Experimental study on rockburst processes of granite specimen at great depth," *Chinese Journal of Rock Mechanics and Engineering*, vol. 26, no. 5, pp. 865–876, 2007.

[9] M. C. He, J. L. Miao, and J. L. Feng, "Rock burst process of limestone and its acoustic emission characteristics under true-triaxial unloading conditions," *International Journal of Rock Mechanics and Mining Sciences*, vol. 47, no. 2, pp. 286–298, 2010.

[10] W. Z. Chen, S. P. Lu, X. H. Guo, and C. J. Qiao, "Unloading confining pressure for brittle rock and mechanism of rock burst," *Chinese Journal of Geotechnical Engineering*, vol. 32, no. 6, pp. 963–969, 2010.

[11] L. S. Xu, "Research on the experimental rock mechanics of rockburst under unloading condition," *Journal of Chongqing Jiaotong University*, vol. 1, pp. 1–4, 2003.

[12] S. F. Wang, L. Q. Huang, and X. B. Li, "Analysis of rockburst triggered by hard rock fragmentation using a conical pick under high uniaxial stress," *Tunnelling and Underground Space Technology*, vol. 96, p. 103195, 2020.

[13] G. S. Su, J. Q. Jiang, X. F. Xia, C. Mo, and Q. Jiang, "Experimental study on ejection process in rockburst," *Chinese Journal of Rock Mechanics and Engineering*, vol. 35, no. 10, pp. 1990–1999, 2016.

[14] H. Zhou, R. C. Xu, J. J. Lu, C. Q. Zhang, F. Z. Meng, and Z. Shen, "Study on mechanisms and physic al simulation experiment of slab buckling rockburst in deep tunnel," *Chinese Journal of Rock Mechanics and Engineering*, vol. 34, no. S2, pp. 3658–3666, 2015.

[15] A. Y. Ma, F. Q. Wu, P. Sha, F. Zhao, and B. C. Sheng, "Progressive failure of Jinping marble in true triaxial rockburst test," *Rock and Soil Mechanics*, vol. 35, no. 10, pp. 2868–2874, 2014.

[16] L. Li, H. M. Jiang, X. B. Chen, and Z. X. Luo, "Model test study on the mechanical mechanism of strain rockbursts," *Chinese Journal of Rock Mechanics and Engineering*, vol. 37, no. 12, pp. 2733–2741, 2018.

[17] C. A. Tang, J. M. Wang, and J. J. Zhang, "Preliminary engineering application of microseismic monitoring technique to rockburst prediction in tunneling of Jinping II project," *Journal of Rock Mechanics and Geotechnical Engineering*, vol. 2, no. 3, pp. 193–208, 2010.

[18] X. T. Feng, B. R. Chen, H. J. Ming et al., "Evolution law and mechanism of rockbursts in deep tunnels: immediate rockburst," *Chinese Journal of Rock Mechanics and Engineering*, vol. 31, no. 3, pp. 433–444, 2012.

[19] X. T. Feng, Y. X. Xiao, G. L. Feng et al., "Study on the development process of rockbursts," *Chinese Journal of Rock Mechanics and Engineering*, vol. 38, no. 4, pp. 649–673, 2019.

[20] T. H. Ma, C. A. Tang, L. X. Tang, W. D. Zhang, and L. Wang, "Rockburst characteristics and microseismic monitoring of deep-buried tunnels for Jinping II hydropower station," *Tunnelling and Underground Space Technology*, vol. 49, pp. 345–368, 2015.

[21] G. L. Feng, X. T. Feng, B. R. Chen, Y. X. Xiao, and Y. Yu, "A microseismic method for dynamic warning of rockburst development processes in tunnels," *Rock Mechanics and Rock Engineering*, vol. 48, no. 5, pp. 2061–2076, 2015.

[22] M. Cai, P. K. Kaiser, H. Morioka et al., "FLAC/PFC coupled numerical simulation of AE in large-scale underground excavations," *International Journal of Rock Mechanics and Mining Sciences*, vol. 44, no. 4, pp. 550–564, 2007.

[23] Z. N. Zhao, X. T. Feng, B. R. Chen, G. L. Feng, and T. Y. Chen, "Study of relativity between rockburst and microseismic activity zone in deep tunnel," *Rock and Soil Mechanics*, vol. 34, no. 2, pp. 491–497, 2013.

[24] B. R. Chen, X. T. Feng, H. J. Ming et al., "Evolution law and mechanism of rockburst in deep tunnel: time delayed rockburst," *Chinese Journal of Rock Mechanics and Engineering*, vol. 31, no. 3, pp. 561–569, 2012.

[25] N. W. Xu, T. B. Li, F. Dai, R. Zhang, C. A. Tang, and L. X. Tang, "Microseismic monitoring of strainburst activities in deep tunnels at the Jinping II hydropower station, China," *Rock Mechanics and Rock Engineering*, vol. 49, no. 3, pp. 981–1000, 2016.

[26] Q. Yu, D. Zhao, Y. Xia et al., "Multivariate early warning method for rockburst monitoring based on microseismic activity characteristics," *Frontiers in Earth Science*, vol. 10, article 837333, 2022.

[27] C. Q. Zhang, X. T. Feng, H. Zhou, S. L. Qiu, and W. P. Wu, "Case histories of four extremely intense rockbursts in deep tunnels," *Rock Mechanics and Rock Engineering*, vol. 45, no. 3, pp. 275–288, 2012.

[28] S. J. Gibowicz, R. P. Young, S. Talebi, and D. J. Rawlence, "Source parameters of seismic events at the Underground Research Laboratory in Manitoba, Canada: scaling relations for events with moment magnitude smaller than-2," *Bulletin of the Seismological Society of America*, vol. 81, no. 4, pp. 1157–1182, 1991.

[29] D. Krajcinovic and M. A. G. Silva, "Statistical aspects of the continuous damage theory," *International Journal of Solids and Structures*, vol. 18, no. 7, pp. 551–562, 1982.

[30] P. Duplancic, *Characterisation of caving mechanisms through analysis of stress and seismicity*, PhD Thesis, University of Western Australia, Perth, Australia, 2001.

[31] M. R. Hudyma, *Analysis and interpretation of clusters of seismic events in mines*, PhD Thesis, University of Western Australia, Perth, Australia, 2008.

[32] Z. H. Hui, L. U. Jing-jing, H. U. Shan-chao, Z. Chuan-qing, X. Rong-chao, and M. Fan-zhen, "Influence of curvature radius of tunnels excavation section on slabbing of hard brittle rockmass under high stress," *Rock and Soil Mechanics*, vol. 37, no. 1, pp. 140–146, 2016.

[33] Z. H. Hui, X. U. Rong-chao, L. U. Jing-jing, Z. Qi-feng, Z. Chuan-qing, and M. Fan-zhen, "Experimental study of

Downloaded from http://pubs.geoscienceworld.org/gsa/lithosphere/article-pdf/doi/10.2113/2022/4135908/5676430/4135908.pdf
by guest

instability destruction and crack propagation characteristics of slab failure model specimen," *Rock and Soil Mechanics*, vol. 36, no. S2, pp. 1–11, 2015.

[34] C. L. Wang, A. X. Wu, and X. H. Liu, *Microseismic Monitoring Prediction and Controlling Technology of Rockburst Hazard in Deep Mining*, Metallurgical Industry Press, Beijing: China, 2013.

[35] F. Dai, B. Li, N. W. Xu, Y. L. Fan, and C. Q. Zhang, "Deformation forecasting and stability analysis of large-scale underground powerhouse caverns from microseismic monitoring," *International Journal of Rock Mechanics & Mining Sciences*, vol. 86, pp. 269–281, 2016.

[36] Y. J. Xia, H. Zhou, C. Q. Zhang, S. H. He, Y. Gao, and P. Wang, "The evaluation of rock brittleness and its application–a review study," *European Journal of Environmental and Civil Engineering*, vol. 26, no. 1, pp. 239–279, 2022.

[37] Y. J. Xia, C. Q. Zhang, H. Zhou et al., "Structural characteristics of columnar jointed basalt in drainage tunnel of Baihetan hydropower station and its influence on the behavior of P-wave anisotropy," *Engineering Geology*, vol. 264, article 105304, no. 264, 2020.

[38] A. Mendecki, *Seismic Monitoring in Mines*, Chapman & Hall, London, 1997.

[39] B. Gutenberg and C. F. Richter, "Frequency of earthquakes in California," *Bulletin of the Seismological Society of America*, vol. 34, no. 4, pp. 185–188, 1944.

[40] A. D. Santis, G. Cianchini, P. Favali, L. Beranzoli, and E. Boschi, "The Gutenberg–Richter law and entropy of earthquakes: two case studies in Central Italy," *Bulletin of the Seismological Society of America*, vol. 101, no. 3, pp. 1386–1395, 2011.

Downloaded from http://pubs.geoscienceworld.org/gsa/lithosphere/article-pdf/doi/10.2113/2022/4135908/5676430/4135908.pdf
by guest